Journal of Advanced Research in Fluid Mechanics and Thermal Sciences

Journal homepage:
https://semarakilmu.com.my/journals/index.php/fluid_mechanics_thermal_sciences/index
ISSN: 2289-7879

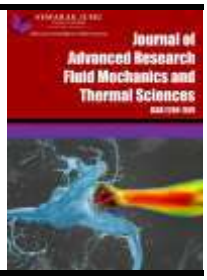

Analytical Solution of the Poiseuille Flow of Second-grade Blood Nanofluid: Comparison of Alumina, Graphene and Copper Nanoparticles

Venkat Rao Kanuri[1,2,*], Venkata Chandra Sekhar Kasulanati[1], Potula Sree Brahmanandam[3], Shyam Sundar Mohan Kumar Medinty[4], Kandarpa Venkata Rama Srinivas[5]

[1] Department of Mathematics, K L University, Vaddeswaram –- 522302, A.P, India
[2] Department of Mathematics, SRKR Engineering College(A), Bhimavaram-534204, A.P, India
[3] Department of Basic Sciences, Shri Vishnu Engineering College for Women(A), Bhimavaram-534202, A.P, India
[4] Department of Humanities and Basic Sciences, Aditya College of Engineering and Technology, Surampalem – 533437, A.P, India
[5] Department of Humanities and Basic Sciences, GIET Engineering College, Rajahmundry – 533297, A.P, India

ARTICLE INFO

Article history:
Received 15 March 2024
Received in revised form 20 June 2024
Accepted 28 June 2024
Available online 15 July 2024

Keywords:
Poiseuille flow; nanofluid; pipe flow; Newtonian flows; analytical solution

ABSTRACT

Poiseuille flows are crucial in various fields, including engineering and the chemical industry, explaining phenomena such as increased blood pressure in narrowed capillaries and aiding in the design of fluid management systems. Traditionally, studies on Poiseuille flows have focused on Newtonian fluids in non-moving pipes, limiting advancements in the field. This research addresses the gap by exploring the Poiseuille flow of a viscoelastic non-Newtonian second-grade nanofluid. These second-grade fluids, applicable in polymer processing and cosmetics manufacturing, exhibit both shear-thinning and shear-thickening properties under certain conditions. The study analytically solves the flow characteristics of blood nanofluids, reducing the governing equations to ordinary differential equations using standard Poiseuille flow assumptions. The simulation results reveal that among the three nanofluids tested, graphene-blood nanofluid achieves the highest velocity, while copper-blood nanofluid exhibits the lowest. Additionally, the velocity of graphene-blood nanofluid decreases with an increase in volume percentage. This work not only advances the understanding of non-Newtonian fluid dynamics but also provides insights into optimizing fluid management systems in biomedical and industrial applications.

1. Introduction

Shear strain responds to shear stress nonlinearly in non-Newtonian fluids. The Casson fluid by Reddy and Reddy [1], Khan *et al.,* [2], and Oke *et al.,* [3], Williamson fluid by Divya *et al.*, [4], Carreau fluid by Murthy and Reddy [5], Eyring –Powell fluid by Oke *et al*., [6], MEP fluid by Oke [7,8] and second-grade fluid by Awan *et al.,* [9] and Krishna *et al.,* [10] are a few examples of these fluids. Second-grade fluids have a second-order relationship between shear stress and shear strain and are classified as non-Newtonian fluids having viscoelastic features. Depending on the particular selection

* *Corresponding author.*
E-mail address: k.ravi.msc@gmail.com

https://doi.org/10.37934/arfmts.119.1.175188

of second-grade fluid, they demonstrate the capacity to shear-thin or shear-thicken. The behaviour of these fluids is governed by both their current condition and their deformation history. Second-grade fluids, which find use in a variety of industrial industries like polymer processing, medicines, and cosmetics, include things like ketchup and blood. A comprehensive study on the Hall slip on unstable MHD flow of second-grade fluids was done by Krishna *et al.,* [10] and the results showed some interesting new uses in aerospace science. Partial differential equations were reformulated to fractional order equations by Yavuz *et al.,* [11], who solved them using the Laplace transform. The findings showed that as the Prandtl number increased, the velocity profile decreased.

Widespread applications involve flows in a range of pipe and channel geometries; these flows are generally categorised as Couette or Poiseuille flows based on the relative movement of the channel walls. A pressure-driven flow is what defines a Poiseuille flow, but a flow between parallel plates moving relative to one another is what defines a Couette flow by Coles [12]. In Poiseuille flow, non-overlapping layers of viscous fluid, known as laminar flow, are sustained by pressure fluctuation according to Gee and Gracie [13]. Poiseuille flow velocity profiles resemble symmetrical parabolas, with no flow on the wall and a maximum point near the middle by Wu *et al.,* [14]. Poiseuille flow is important in the design and development of microfluidic devices because the velocity gradient in this profile improves material transfer. Poiseuille flow has practical uses in a variety of industrial processes, including blood flow through capillaries, in addition to microfluidics. With ramifications for the petroleum industry and other large-scale businesses, it is a useful tool for simulating processes including fluid transport in pipelines, heat exchanger systems, and chemical reactors. It also serves as a means of imitating capillary blood flow by Sulaimon *et al.,* [15], Azmi *et al.,* [16], and Rekha *et al.,* [17]. Poiseuille flow is elegantly solved, which makes it easily transferable to complex medical diagnostics, drug delivery, and microscale chemical analysis.

In this article, a second-grade fluid that flows through a stationary conduit with suspended alumina, copper and graphene nanoparticles is examined. The flow is an extension of the traditional Newtonian Poiseuille flow and represents a Poiseuille nanofluid flow. Existing research extensively covers the behavior of non-Newtonian fluids, focusing on the nonlinear relationship between shear stress and shear strain. Studies have examined various fluids like Casson, Williamson, Carreau, Eyring-Powell, MEP, and second-grade fluids, with second-grade fluids noted for their viscoelastic properties and second-order stress-strain relationship. These fluids are well-studied for applications in polymer processing, pharmaceuticals, and cosmetics. However, there is a significant research gap in understanding second-grade nanofluids, particularly in Poiseuille flow within conduits. The impact of suspended nanoparticles (alumina, copper, graphene) on the flow characteristics of second-grade fluids remains underexplored, where our study has focussed to provide feasible solutions.

In this study, the following queries are addressed

i. How do the flow velocities of graphene-blood nanofluid, alumina-blood nanofluid and copper-blood nanofluid compare?
ii. How does volume fraction impact flow velocity in a second-grade nanofluid flow via a pipe?
iii. How does the flow rate of a second-grade nanofluid pass through a conduit when dynamic viscosity is present?

2. Flow Description and Model Development

Blood, as a second-grade fluid, in which some nanoparticles are suspended flows through a stationary pipe while exhibiting both Newtonian and viscoelastic behaviours. The pipe is considered in a 2D frame so that they are represented as two parallel lines, separated by a distance of $2h$. In this study, the flow entrance region is neglected while the flow is investigated at the region where it is

fully developed. Figure 1 depicts the fully-developed region of the Poiseuille flow with the maximum flow velocity at the centre of the pipe (same as the axis of symmetry $y = 0$). The flow is steady incompressible and laminar.

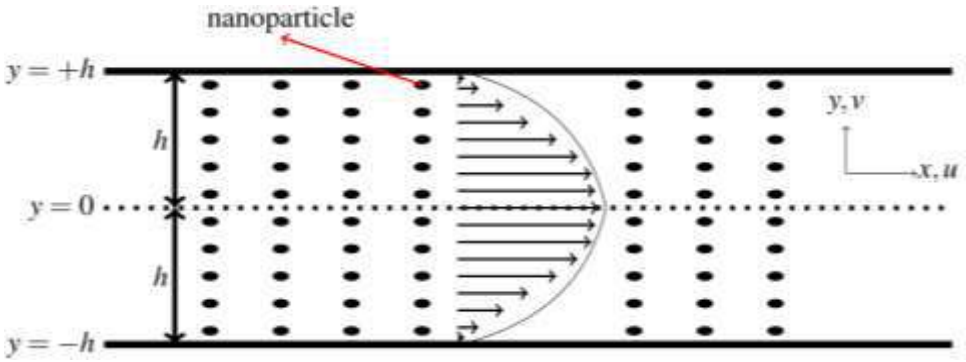

Fig. 1. Flow configuration

The studies by Oke *et al*., [3], Sitamahalakshmi *et al.,* [18], and Kọríkọ *et al.,* [19], suggested the governing equations as

$$\frac{\partial u}{\partial x} + \frac{\partial v}{\partial y} = 0. \tag{1}$$

$$\rho_{nf}\left(u\frac{\partial u}{\partial x} + v\frac{\partial u}{\partial y}\right) = (\nabla \cdot \boldsymbol{\sigma})_x + \rho_{nf} b_x. \tag{2}$$

$$\rho_{nf}\left(u\frac{\partial v}{\partial x} + v\frac{\partial v}{\partial y}\right) = (\nabla \cdot \boldsymbol{\sigma})_y + \rho_{nf} b_y. \tag{3}$$

where u and v are the velocities in the horizontal (x) and vertical (y) axes, $(\nabla \cdot \boldsymbol{\sigma})_x$ and $(\nabla \cdot \boldsymbol{\sigma})_y$ are the shear stress along the x and y directions, b_x and b_y are the body forces in the x and y directions and ρ_{bf} is the nanofluid density. However, Ayub and Zaman [20], Anderson [21], and Beard and Walters [22] provided the stress tensor associated with the second-grade blood fluid as

$$\boldsymbol{\sigma} = -p\boldsymbol{I} + \mu_{nf}\boldsymbol{A}_1 + \alpha_1\boldsymbol{A}_2 + \alpha_2\boldsymbol{A}_1^2. \tag{4}$$

where $\boldsymbol{I}$ is the identity tensor, p is the pressure, μ_{nf} is the dynamic viscosity of the nanofluid, $\boldsymbol{A}_1$ and $\boldsymbol{A}_2$ are the Rivillin Ericksen tensors given as

$$\boldsymbol{A}_1 = \nabla\boldsymbol{V} + (\nabla\boldsymbol{V})^T. \tag{5}$$

$$\boldsymbol{A}_2 = (\boldsymbol{V}\cdot\nabla)\boldsymbol{A}_1 + \boldsymbol{A}_1(\nabla\boldsymbol{V}) + \left(\boldsymbol{A}_1^T(\nabla\boldsymbol{V})\right)^T. \tag{6}$$

The flow equations are therefore written as

$$\frac{\partial u}{\partial x} + \frac{\partial v}{\partial y} = 0. \tag{7}$$

$$u\frac{\partial u}{\partial x} + v\frac{\partial u}{\partial y} = -\frac{1}{\rho_{nf}}\frac{\partial p}{\partial x} + \frac{\mu_{nf}}{\rho_{nf}}\frac{\partial^2 u}{\partial y^2}. \tag{8}$$

$$u\frac{\partial v}{\partial x}+v\frac{\partial v}{\partial y}=-\frac{1}{\rho_{nf}}\frac{\partial p}{\partial y}+\lambda\frac{\partial u}{\partial y}\frac{\partial^2 u}{\partial y^2}. \tag{9}$$

$$0=-\frac{1}{\rho_{nf}}\frac{\partial p}{\partial z}. \tag{10}$$

As shown in the Figure 1 above, there is no flow in the y-direction, indicating that $v=0$ and as a result Eq. (7) reduces to

$$\frac{\partial u}{\partial x}=0. \tag{11}$$

Furthermore, by substituting (11) into (8) – (9), we have

$$0=-\frac{1}{\rho_{nf}}p_x+\frac{\mu_{nf}}{\rho_{nf}}u_{yy}. \tag{12}$$

$$0=-\frac{1}{\rho_{nf}}\frac{\partial p}{\partial y}+\lambda u_y u_{yy}. \tag{13}$$

$$0=-\frac{1}{\rho_{nf}}p_z. \tag{14}$$

2.1 Accompanying Conditions

The walls of the pipe are on the line $y=\pm h$ and the no-slip condition is enforced by allowing the flow velocity to equal the velocity of the pipe. Since the pipe is not moving, then the pipe velocity is zero and consequently, the velocity of the flow is also zero at the pipe walls. This is mathematically represented as

on the upper wall: $y=+h, \quad u=0.$
on the lower wall: $y=-h, \quad u=0.$

Moreover, the physical experiments have shown that there is a stationary point at the centre of the flow, with the stationary point equivalent to the maximum velocity of the flow. It is known from calculus that a stationary point occurs at the point where the derivative is zero, hence, this condition can be represented mathematically as

$$u_y(x,0)=0.$$

2.2 Nanofluid Properties

The fluid properties have been influenced by the inclusion of nanoparticles in the fluid and as a result, the nanofluid properties depend on the properties of the base fluid and that of the nanoparticles included by Animasaun *et al.,* [23]. The nanofluid properties are estimated by Oke *et al.,* [24], and Oke [25] as

$$\mu_{nf}=0.904\mu_{bf}\exp(0.148\phi). \tag{15}$$

$$\rho_{nf} = \left(1 - \phi + \phi \frac{\rho_{np}}{\rho_{bf}}\right)\rho_{bf}. \tag{16}$$

The nanofluids are made up of blood base fluid and each of alumina nanoparticles, graphene nanoparticles and copper nanoparticles. The physical properties of the materials are provided in the Table 1.

Table 1
Comparitive Thermophysical Properties

Material Type	Density $[ML^{-3}]$	Viscosity $[ML^{-1}T^{-1}]$	Source
Blood	1063	3.5-5.5	
Alumina	3970	–	Oke *et al.,* [26]
Graphene	2250	–	Areekara *et al.,* [27]
Copper	8933	–	Ali *et al.,* [28]

2.3 Governing Equations

Making the substitutions (15) and (16) into the Eq. (12) to Eq. (14), the Equations governing the flow becomes

$$0 = -\frac{1}{\left(1-\phi+\phi\frac{\rho_{np}}{\rho_{bf}}\right)\rho_{bf}} p_x + \frac{0.904\mu_{bf}\exp(0.148\phi)}{\left(1-\phi+\phi\frac{\rho_{np}}{\rho_{bf}}\right)\rho_{bf}} u_{yy}, \tag{17}$$

$$0 = -\frac{1}{\left(1-\phi+\phi\frac{\rho_{np}}{\rho_{bf}}\right)\rho_{bf}} \frac{\partial p}{\partial y} + \lambda u_y u_{yy}, \tag{18}$$

$$0 = -\frac{1}{\left(1-\phi+\phi\frac{\rho_{np}}{\rho_{bf}}\right)\rho_{bf}} p_z. \tag{19}$$

Along with the following conditions

$$u(\pm h) = 0 \text{ and } u_y(x, 0) = 0. \tag{20}$$

3. Analytical Solution

The solution to the Eq. (17) to Eq. (19) is obtained in this section for flow velocity and flow rate. The first subsection shows the flow velocity and the second subsection shows the solution of flow rate.

3.1 Exact Flow Velocity

Consider Eq. (19), then

$$-\frac{1}{\left(1-\phi+\phi\frac{\rho_{np}}{\rho_{bf}}\right)\rho_{bf}} p_z = 0\,. \tag{21}$$

$$p_z = 0\,. \tag{22}$$

$$p = p(x, y). \tag{23}$$

and for a cylindrical pipe in 2-dimension, the pressure can be represented as

$$p(x, y) = x^2 + y^2 = h^2. \tag{24}$$

From this point, it is easy to see that

$$\frac{\partial p}{\partial x} = 2x, \quad \frac{\partial p}{\partial y} = 2y, \tag{25}$$

and on substituting the derivatives (25) into the Eq. (17) and Eq. (18), we have

$$0 = -\frac{2x}{\left(1-\phi+\phi\frac{\rho_{np}}{\rho_{bf}}\right)\rho_{bf}} + \frac{0.904\mu_{bf}\exp(0.148\phi)}{\left(1-\phi+\phi\frac{\rho_{np}}{\rho_{bf}}\right)\rho_{bf}} u_{yy}. \tag{26}$$

$$0 = -\frac{2y}{\left(1-\phi+\phi\frac{\rho_{np}}{\rho_{bf}}\right)\rho_{bf}} + \lambda u_y u_{yy}. \tag{27}$$

By rearranging Eq. (26), we have

$$\begin{aligned}
&\frac{0.904\mu_{bf}\exp(0.148\phi)}{\left(1-\phi+\phi\frac{\rho_{np}}{\rho_{bf}}\right)\rho_{bf}} u_{yy} = \frac{2x}{\left(1-\phi+\phi\frac{\rho_{np}}{\rho_{bf}}\right)\rho_{bf}}, \\
&u_{yy} = \frac{2x}{\left(1-\phi+\phi\frac{\rho_{np}}{\rho_{bf}}\right)\rho_{bf}} \div \frac{0.904\mu_{bf}\exp(0.148\phi)}{\left(1-\phi+\phi\frac{\rho_{np}}{\rho_{bf}}\right)\rho_{bf}}, \\
&u_{yy} = \frac{2x}{\left(1-\phi+\phi\frac{\rho_{np}}{\rho_{bf}}\right)\rho_{bf}} \times \frac{\left(1-\phi+\phi\frac{\rho_{np}}{\rho_{bf}}\right)\rho_{bf}}{0.904\mu_{bf}\exp(0.148\phi)}, \\
&u_{yy} = \frac{2x}{0.904\mu_{bf}\exp(0.148\phi)}.
\end{aligned} \tag{28}$$

Put (28) into (27), we have

$$\begin{aligned}
&-\frac{2y}{\left(1-\phi+\phi\frac{\rho_{np}}{\rho_{bf}}\right)\rho_{bf}} + \lambda u_y \frac{2x}{0.904\mu_{bf}\exp(0.148\phi)} = 0, \\
&\lambda u_y \frac{2x}{0.904\mu_{bf}\exp(0.148\phi)} = \frac{2y}{\left(1-\phi+\phi\frac{\rho_{np}}{\rho_{bf}}\right)\rho_{bf}}, \\
&\lambda u_y = \frac{0.904\mu_{bf} y\exp(0.148\phi)}{\left(1-\phi+\phi\frac{\rho_{np}}{\rho_{bf}}\right)x\rho_{bf}}, \\
&u_y = \frac{0.904\mu_{bf} y\exp(0.148\phi)}{\left(1-\phi+\phi\frac{\rho_{np}}{\rho_{bf}}\right)x\lambda\rho_{bf}}.
\end{aligned} \tag{29}$$

Making x the subject from (24), we have

$$x = \sqrt{y^2 - h^2}\,. \tag{30}$$

and therefore,

$$u_y = \frac{0.904\mu_{bf}\exp(0.148\phi)}{\left(1-\phi+\phi\frac{\rho_{np}}{\rho_{bf}}\right)\lambda\rho_{bf}}\frac{y}{\sqrt{y^2-h^2}}\,. \tag{31}$$

On integrating both sides with respect to y, we have

$$u = \frac{0.904\mu_{bf}\exp(0.148\phi)}{\left(1-\phi+\phi\frac{\rho_{np}}{\rho_{bf}}\right)\lambda\rho_{bf}}\int\frac{y}{\sqrt{y^2-h^2}}dy + A. \tag{32}$$

Let $y = h\sin\theta$ so that

$$y^2 - h^2 = h^2\cos^2\theta \quad \Rightarrow \quad \sqrt{y^2-h^2} = h\cos\theta \quad and \quad dy = h\cos\theta\, d\theta$$

$$u = \frac{0.904\mu_{bf}\exp(0.148\phi)}{\left(1-\phi+\phi\frac{\rho_{np}}{\rho_{bf}}\right)\lambda\rho_{bf}}\int\frac{h\sin\theta}{h\cos\theta}h\cos\theta\, d\theta + A,$$

$$u = \frac{0.904\mu_{bf}\exp(0.148\phi)}{\left(1-\phi+\phi\frac{\rho_{np}}{\rho_{bf}}\right)\lambda\rho_{bf}}\int h\sin\theta\, d\theta + A,$$

$$= -\frac{0.904\mu_{bf}\exp(0.148\phi)}{\left(1-\phi+\phi\frac{\rho_{np}}{\rho_{bf}}\right)\lambda\rho_{bf}}h\cos\theta + A,$$

$$= -\frac{0.904\mu_{bf}\exp(0.148\phi)}{\left(1-\phi+\phi\frac{\rho_{np}}{\rho_{bf}}\right)\lambda\rho_{bf}}\sqrt{h^2-y^2} + A.$$

Given that $u(\pm h) = 0$ (from Eq. (20), then

$A = 0$,

And hence,

$$u = -\frac{0.904\mu_{bf}\exp(0.148\phi)}{\left(1-\phi+\phi\frac{\rho_{np}}{\rho_{bf}}\right)\lambda\rho_{bf}}\sqrt{h^2-y^2}. \tag{33}$$

3.2 Exact Flow Rate

The amount of nanofluid that passes through a certain point at any point in time is called the flow rate. The nanofluid flow rate through the pipe $(-h \le y \le +h)$ is defined as

$$q = \int_{y=-h}^{y=+h} u\, dy. \tag{34}$$

Putting Eq. (33) in Eq. (34), we have

$$\begin{aligned} q &= \int_{y=-h}^{y=+h} -\frac{0.904\mu_{bf}\exp(0.148\phi)}{\left(1-\phi+\phi\frac{\rho_{np}}{\rho_{bf}}\right)\lambda\rho_{bf}}\sqrt{h^2-y^2}\, dy, \\ &= -\frac{0.904\mu_{bf}\exp(0.148\phi)}{\left(1-\phi+\phi\frac{\rho_{np}}{\rho_{bf}}\right)\lambda\rho_{bf}}\int_{y=-h}^{y=+h}\sqrt{h^2-y^2}\, dy\,. \end{aligned} \tag{35}$$

Let $y = h\sin\theta$, then $\sqrt{h^2-y^2} = \sqrt{h^2-h^2\sin^2\theta} = h\cos\theta$ and $dy = h\cos\theta\, d\theta$, thus

$$\begin{aligned} q &= -\frac{0.904\mu_{bf}\exp(0.148\phi)}{\left(1-\phi+\phi\frac{\rho_{np}}{\rho_{bf}}\right)\lambda\rho_{bf}}\int_{y=-h}^{y=+h}\sqrt{h^2-y^2}\, dy \\ &= -\frac{0.904\mu_{bf}\exp(0.148\phi)}{\left(1-\phi+\phi\frac{\rho_{np}}{\rho_{bf}}\right)\lambda\rho_{bf}}\int_{\theta=-\frac{\pi}{4}}^{\theta=+\frac{\pi}{4}} h^2\cos^2\theta\, d\theta, \\ &= -\frac{0.904\mu_{bf}\exp(0.148\phi)}{\left(1-\phi+\phi\frac{\rho_{np}}{\rho_{bf}}\right)\lambda\rho_{bf}}\int_{\theta=-\frac{\pi}{4}}^{\theta=+\frac{\pi}{4}} \frac{h^2}{2}(1+\cos 2\theta)\, d\theta, \\ &= -\frac{0.904\mu_{bf}h^2\exp(0.148\phi)}{2\left(1-\phi+\phi\frac{\rho_{np}}{\rho_{bf}}\right)\lambda\rho_{bf}}\int_{\theta=-\frac{\pi}{4}}^{\theta=+\frac{\pi}{4}}(1+\cos 2\theta)\, d\theta, \\ &= -\frac{0.904\mu_{bf}h^2\exp(0.148\phi)}{2\left(1-\phi+\phi\frac{\rho_{np}}{\rho_{bf}}\right)\lambda\rho_{bf}}\left(\theta+\frac{\sin 2\theta}{2}\right)_{\theta=-\frac{\pi}{4}}^{\theta=\frac{\pi}{4}}, \\ &= -\frac{0.904\mu_{bf}h^2\exp(0.148\phi)}{2\left(1-\phi+\phi\frac{\rho_{np}}{\rho_{bf}}\right)\lambda\rho_{bf}}\left(\left(\frac{\pi}{4}+\frac{\sin\left(\frac{\pi}{2}\right)}{2}\right)-\left(-\frac{\pi}{4}+\frac{\sin\left(-\frac{\pi}{2}\right)}{2}\right)\right), \\ &= -\frac{0.904\mu_{bf}h^2\pi\exp(0.148\phi)}{4\left(1-\phi+\phi\frac{\rho_{np}}{\rho_{bf}}\right)\lambda\rho_{bf}}. \end{aligned} \tag{36}$$

4. Simulations and Discussion of Results

In this study, the flow velocity and flow rate are simulated for the second-grade fluid parameter λ, volume fraction ϕ and the pipe radius h. The velocity and flow rate of the nanofluids are compared in section 4.1 to identify the nanoparticle that produces the highest velocity and flow rate. The nanofluid with the highest velocity is further studied in section 4.2. The default values for the parameters are

$$\lambda = 0.2,\ \ \phi = 0.1,\ \ h = 1.$$

4.1 Comparison of the Nanofluids

Figure 2 shows the comparison between the velocity profiles of the three different nanofluids; alumina-blood, graphene-blood and copper-blood nanofluids. The velocity profile for graphene-blood nanofluid is the highest, followed by the alumina-blood nanofluid and lastly, the copper-blood nanofluid. It should be noted that graphene nanoparticle has the lowest density among the three choice nanoparticles. The density, which is the measure of mass of the nanoparticles that occupy 1 unit of volume. Hence, the less the mass, the higher the velocity and consequently, graphene-blood nanofluid has the highest velocity while copper-blood nanofluid has the least velocity (see Figure 2).

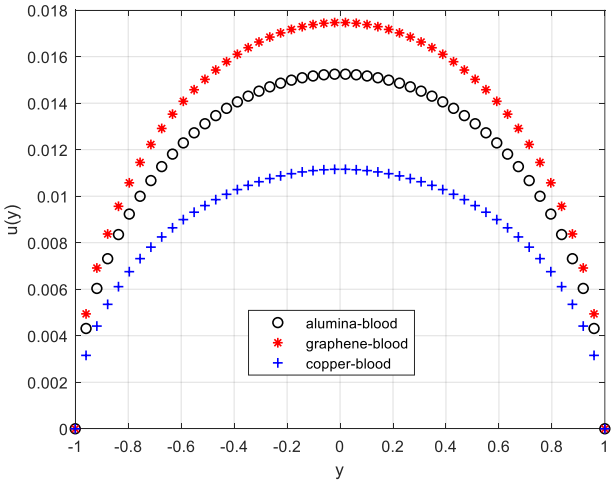

Fig. 2. Velocity comparison for copper, graphene and alumina

Figure 3 illustrates the flow rates of the three nanofluids; graphene-blood nanofluid, alumina-blood nanofluid and copper-blood nanofluid. It can be observed that the graphene-blood nanofluid has the lowest flow rate. This can also be traced to the values of the density of the nanoparticles.

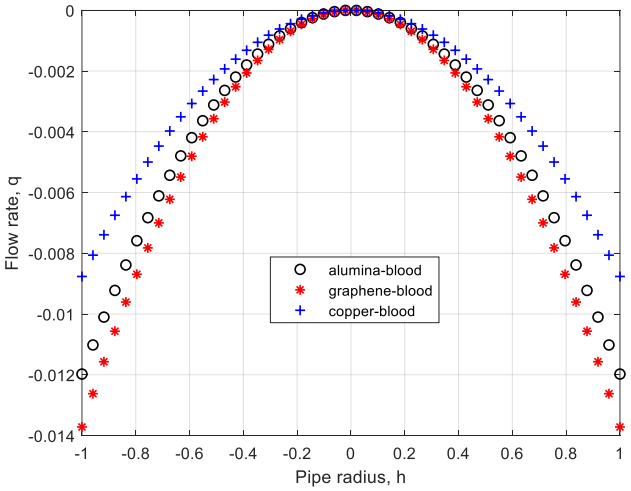

Fig. 3. Flow rate comparison for copper, graphene and alumina

4.2 Behaviour of Graphene-blood Nanofluid

The graphene-blood nanofluid has the highest velocity and lowest flow rate among the three nanofluids, and hence it can enhance heat transfer rate better than the other two nanofluids. The graphene-blood nanofluid is therefore considered in the following analysis and discussions. Figure 4 and Figure 5 describe the velocity of flow and rate of flow as the flow becomes more non-Newtonian. As the material parameter λ grows higher, the fluid migrates farther from Newtonian behaviour and the viscoelasticity of the fluid becomes more pronounced closer to the free stream. Hence, increasing λ increases the drag at the wall, and consequently attempts to drag more fluid layers to a halt. The dragging effect of λ consequently reduces the flow velocity, hence Figure 4 shows the reduction in velocity as λ becomes larger. The flow rate, as shown in Figure 5, increases with increasing λ but decreases as the pipe radius becomes larger. The drag experienced at the wall, with a ripple effect at the free stream, leads to the transfer of more fluid through any cross-sectional area. Meanwhile, the flow rate reduces as the pipe radius increases. Smaller pipe radii result in higher velocity gradients across the cross-section of the pipe. The fluid velocity at the centre of the pipe is higher than that near the walls. This velocity gradient contributes to increased viscous losses and reduced overall flow rate. The flow velocity is studied as the volume fraction increases and the outcomes are shown in Figure 6 and Figure 7. Figure 6 shows that velocity decreases with increasing volume fraction. The volume fraction represents the fraction of the nanofluid occupied by the nanoparticles. The implication of this is that the more the volume fraction, the more the nanoparticles in the nanofluid and the less the base fluid. Clearly, the excess nanoparticles will stick more to the wall and oppose fluid flow. Moreover, checking shows that there is a significant drop in velocity as the volume fraction varies from 0.1 to 0.4 (as can be observed from region A of Figure 6) while the drop in the velocity as the volume fraction varies from 0.8 to 0.9 is very little (region B of Figure 6). Figure 7 shows the variation in the flow rate as the volume fraction increases. The flow rate has an upward trend as the volume fraction increases.

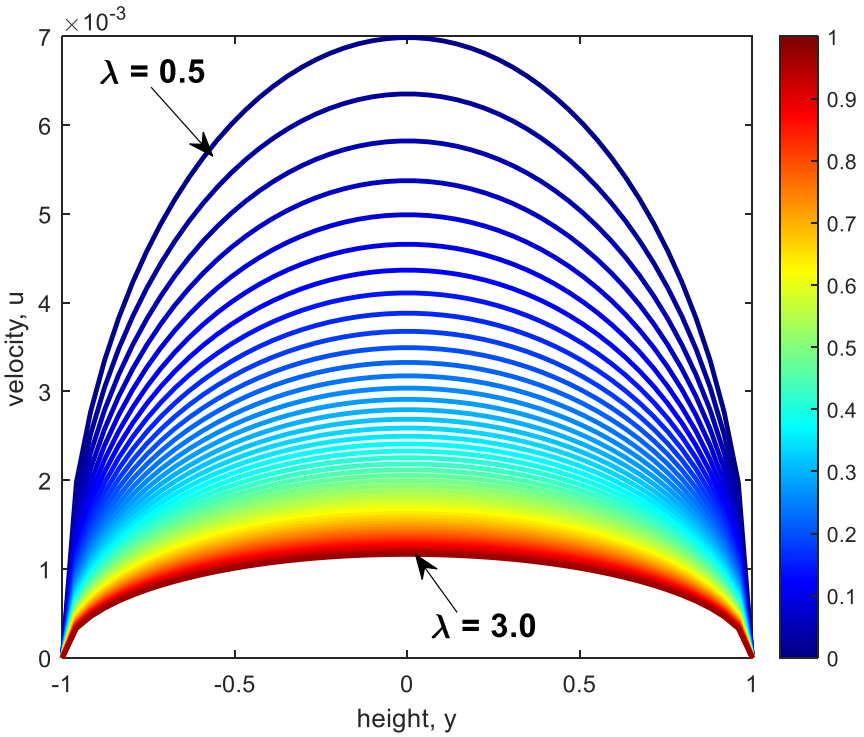

Fig. 4. Velocity variation with increasing **λ**

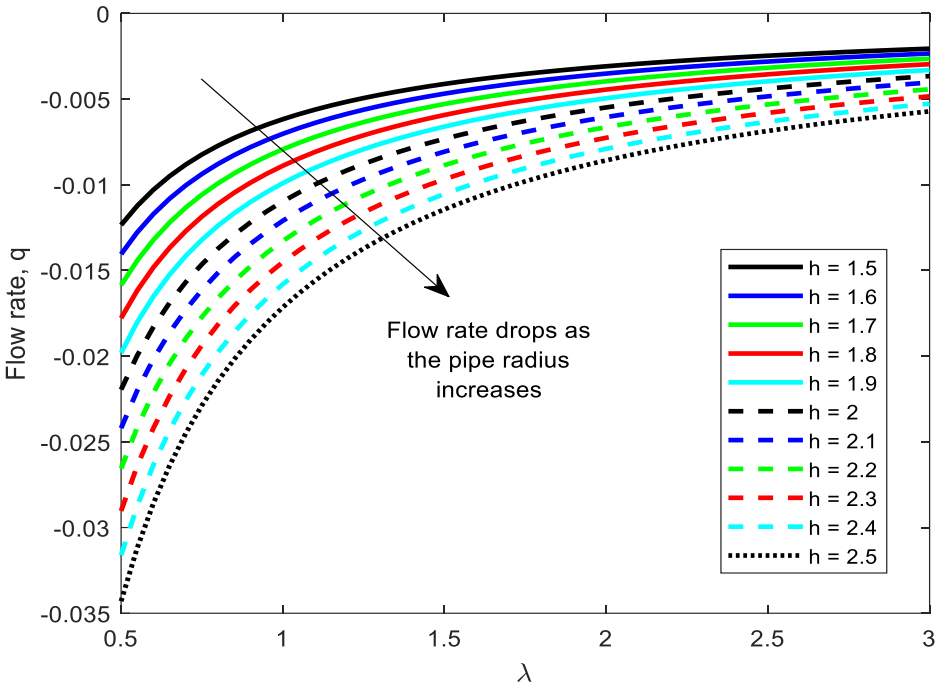

Fig. 5. Flow rate with increasing pipe radius and **λ**

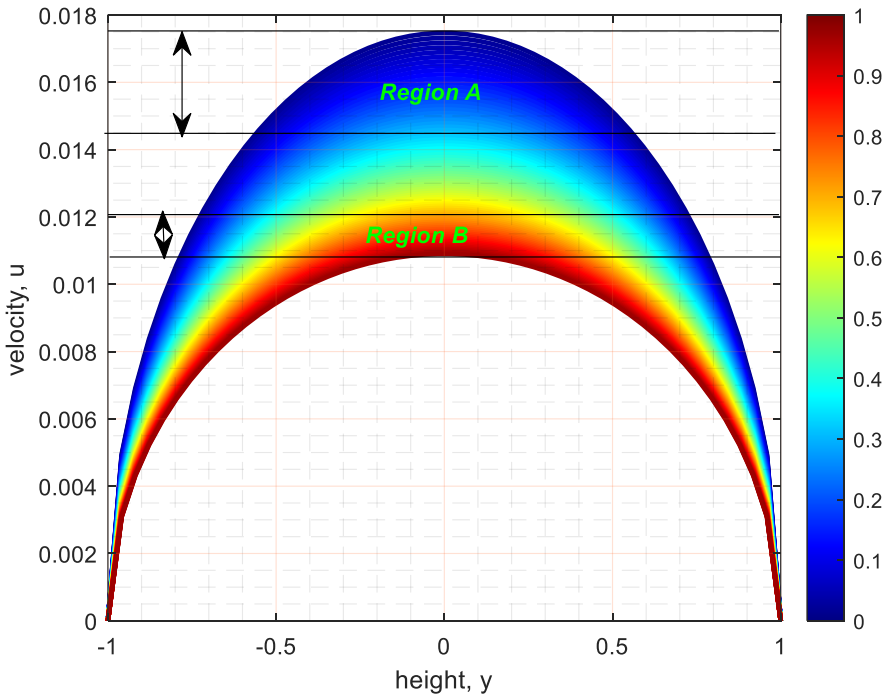

Fig. 6. Velocity variation with increasing **ϕ**

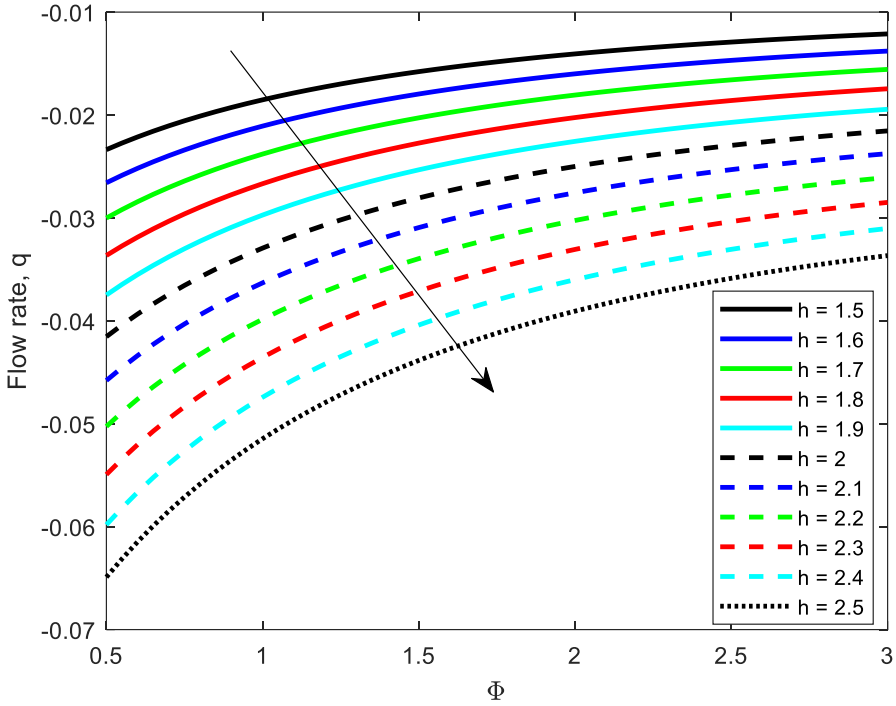

Fig. 7. Flow rate variation with increasing ϕ and pipe radius

5. Conclusions

The Poiseuille flow of nanofluid with blood second-grade base-fluid in a stationary pipe is explored in this study. The pipe is considered to be of diameter $2h$ so that the axis of symmetry is taken as the $y = 0$. A 2-dimensional system of equations is developed for the flow. The exact close form for the velocity profile and the flow rate is obtained as

$$u = -\frac{0.904\mu_{bf}\exp(0.148\phi)}{\left(1-\phi+\phi\frac{\rho_{np}}{\rho_{bf}}\right)\lambda\rho_{bf}}\sqrt{h^2-y^2}\,.$$

$$q = -\frac{0.904\mu_{bf}h^2\pi\exp(0.148\phi)}{4\left(1-\phi+\phi\frac{\rho_{np}}{\rho_{bf}}\right)\lambda\rho_{bf}}.$$

These solutions are simulated to identify the behaviours of the flows of three nanofluids; graphene-blood, copper-blood and alumina-blood nanofluids.

The following are the salient results of the present study.

i. Graphene-blood nanofluid has the highest velocity among the three nanofluids while copper-blood nanofluid has the least velocity.
ii. Graphene-blood nanofluid has the lowest flow rate while copper-blood nanofluid has the highest velocity.
iii. Velocity decreases with increasing volume fraction.
iv. There is a decrease in velocity as the material parameter increases.
v. As the volume fraction increased, the flow rate shown an upward trend.

Acknowledgement
This research was not funded by any grant.

References

[1] Reddy, Karnati Veera, and Gurrampati Venkata Ramana Reddy. "Outlining the impact of melting on mhd casson fluid flow past a stretching sheet in a porous medium with radiation." *Biointerface Research in Applied Chemistry* 13 (2022): 1-14. https://doi.org/10.33263/BRIAC131.042

[2] Khan, Dolat, Poom Kumam, and Wiboonsak Watthayu. "Multi-generalized slip and ramped wall temperature effect on MHD Casson fluid: second law analysis." *Journal of Thermal Analysis and Calorimetry* 147, no. 23 (2022): 13597-13609. https://doi.org/10.1007/s10973-022-11482-6

[3] Oke, Abayomi S., Winifred N. Mutuku, Mark Kimathi, and Isaac L. Animasaun. "Insight into the dynamics of non-Newtonian Casson fluid over a rotating non-uniform surface subject to Coriolis force." *Nonlinear Engineering* 9, no. 1 (2020): 398-411. https://doi.org/10.1515/nleng-2020-0025

[4] Divya, G. Poorna, G. V. Reddy, and P. Bindu. "Unsteady MHD Casson and Williamson nanofluids over a permeable stretching sheet in the presence of thermal radiation and chemical reaction." In *AIP Conference Proceedings*, vol. 2707, no. 1. AIP Publishing, 2023. https://doi.org/10.1063/5.0143359

[5] Murthy, C. V., and G. Reddy. "MHD Casson and Carreau Fluid Flow through a Porous Medium with Variable Thermal Conductivity in the Presence of Suction/Injection." *Journal of Naval Architecture & Marine Engineering* 20, no. 1 (2023).

[6] Oke, Abayomi S., Temitope Eyinla, and Belindar A. Juma. "Effect of Coriolis force on modified Eyring Powell fluid flow." *Journal of Engineering Research and Reports* 24, no. 4 (2023): 26-34. https://doi.org/10.9734/jerr/2023/v24i4811

[7] Oke, A. S. "Coriolis effects on MHD flow of MEP fluid over a non-uniform surface in the presence of thermal radiation." *International Communications in Heat and Mass Transfer* 129 (2021): 105695. https://doi.org/10.1016/j.icheatmasstransfer.2021.105695

[8] Oke, A. S. "Theoretical analysis of modified eyring powell fluid flow." *Journal of the Taiwan Institute of Chemical Engineers* 132 (2022): 104152. https://doi.org/10.1016/j.jtice.2021.11.019

[9] Awan, Aziz Ullah, Fahad S. Al-Mubaddel, Sumble Ahmad, Nadeem Abbas, and Mohammad Mahtab Alam. "Significance of thermal radiation, Lorentz force, and non-Darcian porous medium on the dynamics of second-grade fluid subject to exponential stretching sheet." *Waves in Random and Complex Media* (2022): 1-16. https://doi.org/10.1080/17455030.2022.2111030

[10] Krishna, M. Veera, N. Ameer Ahamad, and Ali J. Chamkha. "Hall and ion slip impacts on unsteady MHD convective rotating flow of heat generating/absorbing second grade fluid." *Alexandria Engineering Journal* 60, no. 1 (2021): 845-858. https://doi.org/10.1016/j.aej.2020.10.013

[11] Yavuz, Mehmet, Ndolane Sene, and Mustafa Yıldız. "Analysis of the influences of parameters in the fractional second-grade fluid dynamics." *Mathematics* 10, no. 7 (2022): 1125. https://doi.org/10.3390/math10071125

[12] Coles, Donald. "Transition in circular Couette flow." *Journal of Fluid Mechanics* 21, no. 3 (1965): 385-425. https://doi.org/10.1017/S0022112065000241

[13] Gee, Bruce, and Robert Gracie. "Beyond Poiseuille flow: A transient energy-conserving model for flow through fractures of varying aperture." *Advances in Water Resources* 164 (2022): 104192. https://doi.org/10.1016/j.advwatres.2022.104192

[14] Wu, Shiwen, Zhihao Xu, Ruda Jian, Siyu Tian, Long Zhou, Tengfei Luo, and Guoping Xiong. "Molecular alignment-mediated stick-slip Poiseuille flow of oil in graphene nanochannels." *The Journal of Physical Chemistry B* 127, no. 27 (2023): 6184-6190. https://doi.org/10.1021/acs.jpcb.3c01805

[15] Sulaimon, Aliyu Adebayo, Muhammad Zaid Sannang, Masooma Nazar, and Azmi Mohd Shariff. "Investigating the effect of okra mucilage on waxy oil flow in pipeline." *Journal of Advanced Research in Fluid Mechanics and Thermal Sciences* 107, no. 2 (2023): 41-49. https://doi.org/10.37934/arfmts.107.2.4149

[16] Azmi, Wan Faezah Wan, Ahmad Qushairi Mohamad, Lim Yeou Jiann, and Sharidan Shafie. "Unsteady natural convection flow of blood Casson nanofluid (Au) in a cylinder: nano-cryosurgery applications." *Scientific Reports* 13, no. 1 (2023): 5799. https://doi.org/10.1038/s41598-023-30129-6

[17] Bali, Rekha, and Bhawini Prasad. "Study of nanoparticle diffusion in capillary-tissue exchange system using Jeffrey nanofluid model: effects of shapes of nanoparticles." *CFD Letters* 15, no. 6 (2023): 130-153. https://doi.org/10.37934/cfdl.15.6.130153

[18] Sitamahalakshmi, V., G. Venkata Ramana Reddy, and Bidemi Olumide Falodun. "Heat and mass transfer effects on MHD Casson fluid flow of blood in stretching permeable vessel." *Journal of Applied Nonlinear Dynamics* 12, no. 1 (2023): 87-97. https://doi.org/10.5890/JAND.2023.03.006

[19] Kọríkọ, O. K., K. S. Adegbie, A. S. Oke, and I. L. Animasaun. "Exploration of Coriolis force on motion of air over the upper horizontal surface of a paraboloid of revolution." *Physica Scripta* 95, no. 3 (2020): 035210. https://doi.org/10.1088/1402-4896/ab4c50

[20] Ayub, Muhammad, and Haider Zaman. "Complete derivation of the momentum equation for the second-grade fluid." *Journal of Mathematics and Computer Science* 1, no. 1 (2010): 33-39. https://doi.org/10.22436/jmcs.001.01.05
[21] Andersson, H. I. "MHD flow of a viscoelastic fluid past a stretching surface." *Acta Mechanica* 95, no. 1 (1992): 227-230. https://doi.org/10.1007/BF01170814
[22] Beard, D. W., and Ken Walters. "Elastico-viscous boundary-layer flows I. Two-dimensional flow near a stagnation point." In *Mathematical Proceedings of the Cambridge Philosophical Society*, vol. 60, no. 3, pp. 667-674. Cambridge University Press, 1964. https://doi.org/10.1017/S0305004100038147
[23] Animasaun, I. L., A. S. Oke, Qasem M. Al-Mdallal, and A. M. Zidan. "Exploration of water conveying carbon nanotubes, graphene, and copper nanoparticles on impermeable stagnant and moveable walls experiencing variable temperature: Thermal analysis." *Journal of Thermal Analysis and Calorimetry* 148, no. 10 (2023): 4513-4522. https://doi.org/10.1007/s10973-023-11997-6
[24] Oke, A. S., I. L. Animasaun, W. N. Mutuku, M. Kimathi, Nehad Ali Shah, and S. Saleem. "Significance of Coriolis force, volume fraction, and heat source/sink on the dynamics of water conveying 47 nm alumina nanoparticles over a uniform surface." *Chinese Journal of Physics* 71 (2021): 716-727. https://doi.org/10.1016/j.cjph.2021.02.005
[25] Oke, Abayomi Samuel. "Heat and mass transfer in 3D MHD flow of EG-based ternary hybrid nanofluid over a rotating surface." *Arabian Journal for Science and Engineering* 47, no. 12 (2022): 16015-16031. https://doi.org/10.1007/s13369-022-06838-x
[26] Oke, Abayomi S., Ephesus O. Fatunmbi, Isaac L. Animasaun, and Belindar A. Juma. "Exploration of ternary-hybrid nanofluid experiencing Coriolis and Lorentz forces: case of three-dimensional flow of water conveying carbon nanotubes, graphene, and alumina nanoparticles." *Waves in Random and Complex Media* (2022): 1-20. https://doi.org/10.1080/17455030.2022.2123114
[27] Areekara, Sujesh, A. S. Sabu, Alphonsa Mathew, and A. S. Oke. "Transport phenomena in Darcy-Forchheimer flow over a rotating disk with magnetic field and multiple slip effects: modified Buongiorno nanofluid model." *Waves in Random and Complex Media* (2023): 1-20. https://doi.org/10.1080/17455030.2023.2198611
[28] Ali, Bagh, N. Ameer Ahammad, Aziz Ullah Awan, Abayomi S. Oke, ElSayed M. Tag-ElDin, Farooq Ahmed Shah, and Sonia Majeed. "The dynamics of water-based nanofluid subject to the nanoparticle's radius with a significant magnetic field: The case of rotating micropolar fluid." *Sustainability* 14, no. 17 (2022): 10474. https://doi.org/10.3390/su141710474